First-principles analysis of the interplay between electronic structure and volume change in colquiriite compounds during Li intercalation

A. F. Baumann,[1,*] D. Mutter,[2] D. F. Urban,[1,2] and C. Elsässer[1,2]
[1]*University of Freiburg, Freiburg Materials Research Center (FMF), 79104 Freiburg, Germany*
[2]*Fraunhofer IWM, 79108 Freiburg, Germany*

(Received 30 June 2023; revised 28 September 2023; accepted 5 October 2023; published 23 October 2023)

A main source of capacity fading in lithium-ion batteries is the degradation of the active cathode materials caused by the series of volume changes during charge and discharge cycles. The quaternary colquiriite-type fluorides Li_xCaFeF_6 and Li_xCaCoF_6 were reported to have negligible volume changes in specific Li concentration ranges, making the underlying colquiriite structure a promising candidate for so-called *zero-strain* behavior. Using first-principles electronic structure calculations based on density functional theory with a Hubbard-U correlation correction on the transition-metal ions, we systematically investigate the equilibrium volumes of the colquiriite-type fluorides Li_xCaMF_6 with M = Ti, V, Cr, Mn, Fe, Co, and Ni at the Li concentrations $x = 0$, 1, and 2. We elucidate the connection between the total volume of the structures and the local volumes of fluorine coordinated octahedra around the cations, and we find trends along the series of the *3d* transition-metal elements. In the lithiation step from $x = 1$ to $x = 2$ we find volume changes of about 10%, and we discuss the discrepancy to the experimentally reported smaller value for Li_xCaFeF_6. The suitability as cathode material was furhter investigated by calculating the theoretical voltages and capacities. From $x = 0$ to $x = 1$ we describe the compensating structural mechanisms that lead to an exceptionally small volume change of Li_xCaMnF_6, which posseses a high theoretical voltage and moderate capacity. This compound is therefore a particularly promising zero-strain cathode material.

DOI: 10.1103/PhysRevB.108.165140

I. INTRODUCTION

Active cathode materials for lithium-ion batteries (LIBs) often suffer from mechanical degradation during charge and discharge cycles [1–4]. Among other effects, phase transformations or changes in the lattice parameters can occur as a consequence of the intercalation and deintercalation of Li ions. The associated volume change varies from material to material. The widely used cathode material Li_xCoO_2 (LCO), for example, undergoes a sequence of three distinct phase transitions during delithiation [5]. The associated structural changes were found to be primarily responsible for the performance degradation of graphite/LCO LIBs [6]. So-called *zero-strain* (ZS) materials are characterized by very small volume changes during ionic charging and discharging and are therefore promising candidates for mechanically stable cycling. This is especially relevant in the context of all-solid-state LIBs, where the stability of the interfaces between the active electrode and the solid electrolyte particles is crucial [7,8].

Several ZS materials were reported in the literature and different mechanisms were proposed to explain the effect. $Li_4Ti_5O_{12}$ is a well-known ZS anode material [9–11] for which the ZS behavior can be explained by the compensation of changing O-Ti-O bond angles and Li-O bond lengths during (dis-)charging [12]. Experimentally characterized metal-oxide ZS cathode materials for LIBs include the spinel-type compounds $LiCoMnO_4$, where the ZS behavior is mainly ascribed to a small difference in the ionic radii of Co^{3+}/Co^{4+} [13] and $Li_2Ni_{0.2}Co_{1.8}O_4$, where the effects of contracting Co-O bonds and distortions of the oxygen sublattice cancel each other [14]. In the disordered rocksalt-type Li-excess compounds $Li_{1.3}V_{0.4}Nb_{0.3}O_2$ and $Li_{1.25}V_{0.55}Nb_{0.2}O_{1.9}F_{0.1}$, the ZS behavior is described by effects including the existence of transition-metal redox centers and electrochemical inactive elements and a migration of Li from octahedral to tetrahedral sites [15].

In addition to oxide compounds, ZS behavior has also been observed for some fluoride compounds. In the tungsten-bronze-type compound $K_{0.6}FeF_3$ nearly zero-strain sodiation was measured, which was attributed to the proper size of the cavities for Na ions in this open framework structure [16]. Koyama *et al.* first reported a compound crystallizing in the so-called *colquiriite* structure in the context of ZS positive-electrode materials. With density functional theory (DFT) calculations in the local density approximation (LDA) without spin polarization, they obtained a volume change for Li_xCaCoF_6 of 0.4% for a change of the Li concentration from $x = 1$ to $x = 0$. They explained the ZS behavior during delithiation by the reduction of Co-F bond lengths (due to the oxidation of Co) compensating the elongation of Li-F bond lengths (stronger F^--F^- repulsion due to the missing attraction between Li^+ and F^- after the removal of Li) [17]. De Biasi and coworkers measured a small volume change below 0.5% in the colquiriite-type compound Li_xCaFeF_6 in a

*aljoscha.baumann@fmf.uni-freiburg.de

Li concentration range of $1.0 \leqslant x \leqslant 1.8$ [18]. This small volume expansion was attributed to the large absolute volume of the Li-F octahedron that mitigates the effect of the expanding Fe-F octahedron.

The colquiriite structure is named after the mineral $LiCaAlF_6$, which was first found in Colquiri, Bolivia. Since then, many other compounds with this structure and the general formula $LiA^{2+}M^{3+}F_6$ were successfully synthesized [18–25]. Most research focusing on colquiriites concerns their application as laser media. Especially Cr-doped $LiCaAlF_6$ and $LiSrAlF_6$ were investigated both experimentally and theoretically [26–30].

Pawlak *et al.* investigated the correlation between structural parameters of colquiriite structures by means of a statistical analysis of available experimental data [31]. For a set of $LiCaMF_6$ structures they showed that different M ions have a strong influence on both lattice parameters a and c as well as on the Li-F bond length: With larger M-F bond lengths the Li(2c)-F bond length increases, too. However, no structural correlation was detected between the M-F and Ca-F bond lengths.

Motivated by the stability of the crystalline colquiriite framework for various element combinations on the cation sublattices, and by the reports of ZS behavior for representatives of this structure type, we apply electronic structure calculations to systematically analyze the volume changes of the colquiriite compounds Li_xCaMF_6 for the lithiation steps from $x = 0$ to $x = 1$ and from $x = 1$ to $x = 2$, considering the series of $3d$ transition-metal elements (TMs) Ti, Cr, V, Mn, Fe, Co, and Ni on the M site. We investigate different magnetic configurations of the TM $3d$ electrons since these influence the total energy and volume of the compounds. Electronic structure calculations are a valuable tool to study volume effects related to magnetism in metals. Previous reports that relate the electronic structure to volume effects include, e.g., the so-called Invar effect [32], the relationship between magnetism and volume of cubic Fe, Co, and Ni phases [33] and magnetovolume effects in iron and cobalt nitrides [34].

The paper is organized as follows: In Sec. II A, the colquiriite structure is described, followed by a description of the computational details in Sec. II B. The results of the atomistic DFT calculations for the determination of the magnetic ground states are presented in Sec. III A and the volume changes between those states for different Li concentrations are presented in Sec. III B. The results are discussed in Sec. IV: First we compare ionic radii for different U values (IV A), then we discuss the relationship between the changes in ionic radii (viz. volumes of octahedra) during lithiation and the electronic structure of the TM element (IV B), followed by an explanation of how the local volumes of octahedra of fluorine anions determine the total unit-cell volume of the crystal structure (IV C). Our conclusions are given in Sec. V.

II. THEORETICAL APPROACH

A. Colquiriite structure

Colquiriite-type compounds crystallize in the trigonal space group $P\bar{3}1c$. The unit cell of a $LiCaMF_6$ crystal consists of two formula units (f.u.), i.e., 18 atoms, displayed in

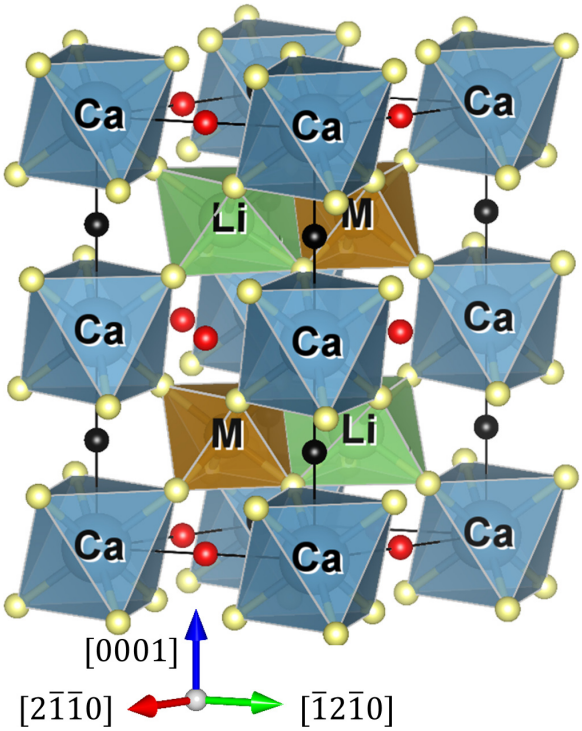

FIG. 1. Trigonal unit cell of the colquiriite-type structure of $LiCaMF_6$ (M = Ti, V, Cr, Mn, Fe, Co, and Ni). The octahedra of M cations coordinated by fluorine anions (yellow spheres) are labeled by the respective central cation M. Black and red spheres at Wyckoff positions 2a and 6g, respectively, indicate the possible sites for additional Li ions.

Fig. 1. The lattice parameter a is defined along the $[2\bar{1}\bar{1}0]$ direction (or equivalently along the $[\bar{1}2\bar{1}0]$ direction) and c is defined along the [0001] direction. Along the [0001] direction, the crystal consists of alternating layers of fluorine coordinated Ca and Li/M octahedra. The Ca and M ions occupy the Wyckoff positions (WPs) 2b and 2d, respectively. If there is one Li atom per f.u., then it is located at the WP 2c. Additional possible sites for Li ions in the case of higher Li concentrations are the WPs 2a and 6g (fractional coordinates: [0, 0, 1/4] and [0, 1/2, 1/2], where for the latter, three inequivalent arrangements of Li ions on these sites are possible). We describe the energetic hierarchy of the different Li occupations in more detail in Sec. III A 1. Table I lists the coordinates of the symmetric sites of the colquiriite structure.

TABLE I. Wyckoff positions and fractional coordinates of the asymmetric unit of the colquiriite structure (space group $P\bar{3}1c$). The fluorine atoms, which occupy the general position $[x, y, z]$ are here exemplarily given for $LiCaAlF_6$ according to Ref. [35].

Atom	Multiplicity	Wyckoff letter	x	y	z
Ca	2	b	0	0	0
Li	2	c	1/3	2/3	1/4
M	2	d	2/3	1/3	1/4
F	12	i	0.376	0.032	0.144

B. Computational details

We determine the equilibrium volumes V_0 of the colquiriite unit cells by fitting the Murnaghan equation of state (EOS) [36] to a dataset of minimal total energies calculated for different unit-cell volumes. At each given volume we optimize the unit-cell shape and the atomic coordinates.

The procedure of using energy-volume (EV) curves [37,38] gives more accurate results for V_0 compared to the volume optimization by stress minimization, with routines implemented in most atomistic simulation codes. It avoids numerical errors in the Pulay stresses that originate from the dependence of the incompleteness of the plane-waves basis on the unit-cell volume. In addition, by means of the EV curves, one can clearly distinguish minimum energies and equilibrium volumes of electronically or magnetically stable (ground-state) and metastable structures as long as those follow separate EV curves rather than only getting one–global or local–energy-minimum point as in the case of unconstrained volume optimization by stress minimization.

All DFT calculations were carried out with the Vienna ab initio simulation package [39]. The Perdew-Burke-Ernzerhof generalized gradient approximation [40] was used for the exchange-correlation functional. Interactions between valence electrons and ionic cores are treated with the projector-augmented wave method [41]: For Li, the 1s, 2s, and 2p orbitals; for Ca, the 3s, 3p, and 4s orbitals; for the considered TMs, the 3s, 3p, 3d, and 4s orbitals; and for F, the 2s and 2p orbitals are taken as valence states.

Similarly to the situation in oxides, the localized electrons of the 3d TMs in fluorides are often not well described by DFT with LDA or GGA approximations. A Hubbard-U correlation-correction term can mitigate the respective self-interaction error which leads to a too-weak localization of the 3d electrons [42–48]. The value of the U parameter is often chosen semiempirically, e.g., by tuning it to match the calculated electronic band gap with experimentally measured values. However, the scarce experimental data for the electronic structure of colquiriite-type fluoride compounds, especially for the band gap, does not allow a corresponding adjustment of the U value for our study. We therefore pursue a more generic comparison between theoretically calculated and experimentally measured quantities: We compare the change in the ionic radii of the electrochemically active cations during lithiation, extracted from the ground-state structures for different U values, to the change in the ionic radii given by Shannon [49]. U is chosen in such a way that our calculated values and the Shannon radii match best for the considered series of 3d TM ions. We followed the DFT+U approach of Dudarev *et al.* [50] and compared calculations with values of $U_{\text{eff}} = 0$ (no U correction), 4, and 8 eV on the 3d orbitals of the M ions, where $U_{\text{eff}} = U - J$. Here U denotes the on-site Coulomb term and J the site exchange term. To simplify the notation, U_{eff} will be denoted just as U in the following.

We set the energy cutoff for the plane-waves basis to 700 eV and use a 6×6×3 Monkhorst-Pack [51] k-point mesh with a Gaussian smearing of 0.05 eV [52,53] for the Brillouin-zone integrations. We converged the total energies to 5×10^{-6} eV in the electronic self-consistency loop and the interatomic forces to 0.05 eV/Å in the ionic relaxation loop.

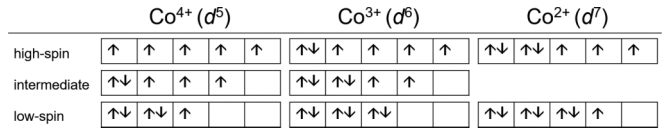

FIG. 2. Possibilities to distribute the 3d electrons of Co in the 3d orbitals for three different oxidation states. The arrows indicate the two different spin directions of the electrons. The corresponding local magnetic moments of the ions are obtained by counting the unpaired electrons.

III. RESULTS

A. Ground-state configurations

In order to find the state of lowest energy (ground state) for each considered compound Li_xCaMF_6, we investigated the different possible sites for Li ions in the colquiriite structure and the different possible local magnetic moments of the M ions. We then calculated the relative energetic ordering of those compounds.

1. Occupation of Li sites

To figure out which of the WPs 2a, 2c, and 6g are favored to be occupied by Li for the Li concentrations $x = 1$ and $x = 2$, we set up the corresponding unit cells and calculated the EV curves. In addition, we deliberately displaced the Li atoms slightly from their high-symmetry WPs, which, however, always resulted in a relaxation back to the WPs. For each crystal composition with TM element M and Li concentration x, the energies of the structures with different Li occupations were calculated for the three considered U values, 0, 4, and 8 eV, and for the possible variety of magnetic states (i.e., high-spin and low-spin states, which are described in detail in Sec. III A 2). In the first lithiation step from $x = 0$ to $x = 1$, we found that the 2c sites are always the energetically favored positions for Li by at least 0.28 eV/f.u.

For the second lithiation step from $x = 1$ to $x = 2$, we accordingly considered unit cells with Li on the 2c sites and placed the two additional Li atoms on the 2a or 6g sites. It turned out that an occupation of the 2a sites leads to structures that are lower in energy by at least 0.11 eV/f.u. than the structures where the 6g sites are occupied.

2. Local magnetic moments of TM ions

Following the idealized chemical notion of occupying atomic orbitals with electrons/spins, there are several distinct possibilities to formally distribute the valence electrons of a TM ion on the atomic 3d orbitals, which lead to different local magnetic moments. Figure 2 exemplary illustrates this for the Co ion in the three oxidation states, Co^{4+}, Co^{3+}, and Co^{2+}. Without considering the corresponding energies, one can in principle distinguish a *high-spin* (HS) state with a maximum number of unpaired electrons, a *low-spin* (LS) state with a minimum number of unpaired electrons, and a state with an intermediate spin configuration. Co has the valence electron configuration $3d^7 4s^2$. With the 4s electrons taken first by fluorine anions, this leads to magnetic moments of 5 μ_B (HS) and 1 μ_B (LS) for Co^{4+}, 4 μ_B (HS) and 0 μ_B (LS) for Co^{3+}, and 3 μ_B (HS) and 1 μ_B (LS) for Co^{2+}, as sketched in Fig. 2.

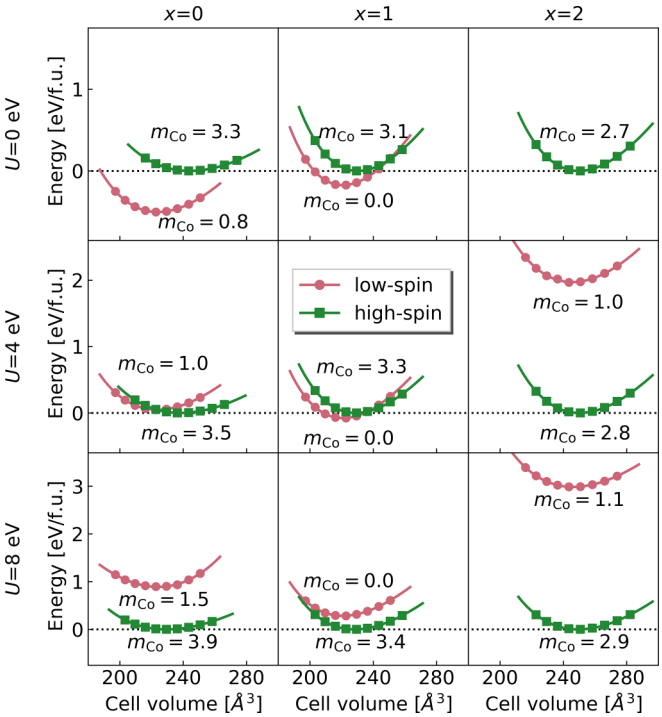

FIG. 3. EV curves of Li_xCaCoF_6 for the three Li concentrations ($x = 0$, 1, and 2) and for the three U parameters ($U = 0$, 4, and 8 eV). In each of the nine panels, the energy is referenced to the energy minimum of the high-spin (HS) EV curve. Filled circles mark calculated total energies per f.u. obtained at fixed volumes and variable cell shape, and solid lines indicate the fitted EOS. The magnetic moments (in units of μ_B) of the Co ions after relaxation are given at each curve.

The three oxidation states 4+, 3+, and 2+ will be considered in the following for each M cation, since they are formally adopted by those ions in the colquiriite structures with Li concentrations $x = 0$, 1, and 2, respectively, as a consequence of total charge neutrality.

For all compounds, we carried out a series of DFT calculations by initializing the magnetic moments at all integer values between 0 μ_B and 5 μ_B. After the structural relaxations, at most two states were found to be stable, namely one HS and one LS state. No initially prepared intermediate state could be stabilized finally. For Ti^{4+}, there is no 3d electron, and for Ti^{3+} and V^{4+}, there is only one 3d electron and hence only a single-spin state. For some cations with more than one 3d electron, i.e., where formally more than one spin state may be expected, only one spin state was found to be stable (e.g., a HS state of V^{2+} with three unpaired 3d electrons and 3 μ_B).

Since there are two M atoms in the unit cell of the colquiriite structure considered in this work, one can distinguish two collinear arrangements of magnetic moments, a ferromagnetic (FM) one, where the local magnetic moments on the two M ions are oriented parallel to each other, and an antiferromagnetic one (AFM), where the local magnetic moments are oriented antiparallel. For the example of Li_xCaCoF_6, we set up the two arrangements with different initial magnetic moments and performed total energy calculations for structures with $x = 0$, 1, and 2, and $U = 0$, 4, and 8 eV. The local magnetic moments of the HS and LS states on the individual M ions were found to be identical for both FM and AFM arrangements, with differences in energy between those of less than 0.0074 eV/f.u. Similar results for other exemplarily tested compounds indicate negligibly weak exchange interactions between the local magnetic moments on the different M ions. Therefore, we present only the results for FM arrangements in the following.

Figure 3 displays the calculated energy versus volume data and the fitted EV curves for $x = 0$, 1, and 2, and for $U = 0$, 4, and 8 eV for Li_xCaCoF_6. The results for HS and LS states are displayed in green and red, respectively. For Li_2CaCoF_6 calculated with $U = 0$ eV, only one magnetic state was stable after relaxation. For the other cases, the energy ordering between HS and LS states depends on the value of U as well as on the Li concentration x. As described above, the additional Li reduces the TM cation which results in different distributions of the 3d electrons with different energies. The magnetic moments increase in magnitude with higher values of U as expected since U forces the electrons to their respective M sites. For the HS states, the calculated values of the magnetic moments are less than the formally expected integer numbers (5 μ_B, 4 μ_B, and 3 μ_B for $x = 0$, 1, and 2, respectively) but approach them for increasing x. The magnetic moments of the M ions in the LS states correspond well to the formal oxidation numbers (0, 1, 0 for $x = 0$, 1, 2). The magnetic moments of all TM ions are reported in the supplemental material [54].

We extract two quantities from each EV curve: (i) the equilibrium energy, E_0, from which we can calculated $\Delta E_0^{\mathrm{HL}} = E_0^{\mathrm{HS}} - E_0^{\mathrm{LS}}$; the difference in minimum energy between the HS and LS state for each combination of x and U; and (ii) the equilibrium volumes V_0 of the ground states at the different Li concentrations x. From those volumes we can calculate ΔV_0, the volume change of the unit cell due to the Li addition.

Table II summarizes the magnetic ground states for all the studied Li_xCaMF_6 compounds and different U values together with ΔE_0^{HL}, where applicable. For M = Ti at $x = 0$ (Ti^{4+}) and $x = 1$ (Ti^{3+}) and for M = V at $x = 1$ (V^{4+}), only a zero-spin or a single-spin state is possible, as explained above and therefore no distinction between LS or HS is meaningful.

For most of the compositions, the HS state is preferred. The LS state was only found to be more stable in some cases containing Co^{3+}/Co^{4+} or Ni^{3+}/Ni^{4+} and with specific values of U.

Our findings for TM fluorides are in good agreement with the findings for TM oxides reported by Jia *et al.* [55], who have analyzed the distribution of magnetic moments of the 3d TM ions, which were calculted by first principles for a large set of compounds from the Materials Project database [56]. For Ti, V, Cr, Mn, and Fe the magnetic moments corresponding to the HS states were the ones occurring most often. For some oxidation states of Co and Ni no clear preferred spin state was found. In the fluoride compounds calculated in this work, for Co^{4+} and the U values $U = 4$ eV and $U = 8$ eV the HS spin state was the energetically favorable one, whereas this state was not found for oxides by Jia *et al.* [55]. They found for Ni^{3+} the low-spin and intermediate-spin state most often, which goes well in line with the experimental findings that Ni^{3+} in $LiNiO_2$ is considered to be in the LS state [57].

TABLE II. Magnetic ground states for the compounds Li_xCaMF_6 with M = Ti, V, Cr, Mn, Fe, Co, and Ni for $x = 0$, 1, and 2 (corresponding to the formal oxidation states of the M cations 4+, 3+, and 2+) and for $U = 0$, 4, and 8 eV applied to the M ions. In parentheses ΔE_0^{HL} is given. (*) indicates that only the magnetic state presented in the table was stable after relaxation. All numerical values are given in eV.

	Ti	V	Cr	Mn	Fe	Co	Ni
$x = 0$; M^{4+}							
$U = 0$			HS (−0.95)	HS (*)	HS (−0.75)	LS (0.5)	LS (*)
$U = 4$			HS (−2.5)	HS (*)	HS (−1.99)	HS (−0.05)	LS (1.0)
$U = 8$			HS (*)	HS (*)	HS (−3.53)	HS (−0.89)	LS (0.13)
$x = 1$; M^{3+}							
$U = 0$		HS (−0.99)	HS (*)	HS (−1.66)	HS (−1.11)	LS (0.17)	LS (*)
$U = 4$		HS (*)	HS (*)	HS (−2.43)	HS (−1.96)	LS (0.08)	HS (−0.26)
$U = 8$		HS (*)	HS (*)	HS (−2.73)	HS (*)	HS (−0.28)	HS (−0.48)
$x = 2$; M^{2+}							
$U = 0$	HS (*)	HS (*)	HS (−1.59)	HS (−2.33)	HS (−1.4)	HS (*)	HS (−1.17)
$U = 4$	HS (*)	HS (*)	HS (−2.2)	HS (*)	HS (−1.81)	HS (−1.97)	HS (*)
$U = 8$	HS (*)	HS (*)	HS (−2.71)	HS (*)	HS (−2.06)	HS (−2.98)	HS (*)

Other DFT + U studies with a wide range of applied U values (2.45 eV [58], 5.96 eV [59], and 3, 6, and 9 eV [60]) agree with that. In the colquiriite fluorides calculated in this work, we found the LS state of Ni^{3+} only for $U = 0$ and otherwise the HS state. Therefore, in general, the preferred spin state depends strongly on the oxidation state of the TM ions and only for some cases the magnetic ground state is influenced by the type of ligand surrounding the TM ion or the applied U value. A trend can be observed that the HS states become more stable with higher U values. This was reported earlier for Fe^{2+} compounds by Mariano *et al.* [61], who calculated the energy differences between HS and LS states for six molecular complexes with different ligands applying DFT + U with U values between 0 and 8 eV.

B. Local and global volume changes

From the obtained crystal structures of the U-dependent magnetic ground states we now analyze the ionic radii of the M cations as function of the Li concentration. We compare the results to Shannon's empirical set of ionic radii extracted from experimental mineral-structure data. This comparison enables us to select a value for U which fits best to experimental structure data. This procedure is discussed in more detail in Sec. IV A. Overall, we found that $U = 4$ eV gives the best agreement (within the values examined in this work) of our and Shannon's radii for both lithiation steps. Therefore, we use this particular U value with good confidence for all the calculations described in the following.

Figure 4 depicts the absolute volumes of fluorine octahedra around the M, Li, and Ca cations. Along the 3d series the MF_6 octahedron volume decreases, which can be explained by the increasing nuclear charge of the atoms. The calculated octahedra volumes follow qualitatively similar trends as the experimentally measured bond lengths reported by Pawlak *et al.* [31] for colquiriite compounds of the type $LiCaMF_6$: Together with a lower MF_6 octahedron volume (lower M-F bond length) the LiF_6 (2c) octahedron volume (Li-F bond length) also decreases and the CaF_6 octahedra volumes are not correlated with the M-F bond lengths.

The experimental results from de Biasi *et al.* [18] for the octahedra volumes are shown for the lithiation concentrations $x = 1$ and $x = 2$. It is important to note that the maximal concentration that was achieved in the experiments was $x = 1.79$. The ^{57}Fe Mössbauer spectroscopy at that concentration, however, showed that most of the iron ions were in the oxidation state Fe^{2+}, i.e., similarly to the oxidation state of the iron ions in the $x = 2$ calculations of this work. In the experimental work only the average value of the LiF_6 octahedra at $x = 1.79$ was reported.

The value for the CaF_6 octahedra volume measured experimentally is closer to the value obtained in the calculations at the lithium concentration $x = 2$ than at $x = 1$. De Biasi *et al.* reported no change in the volume of these octahedra. The values for the FeF_6 and LiF_6 (2c) octahedra volumes

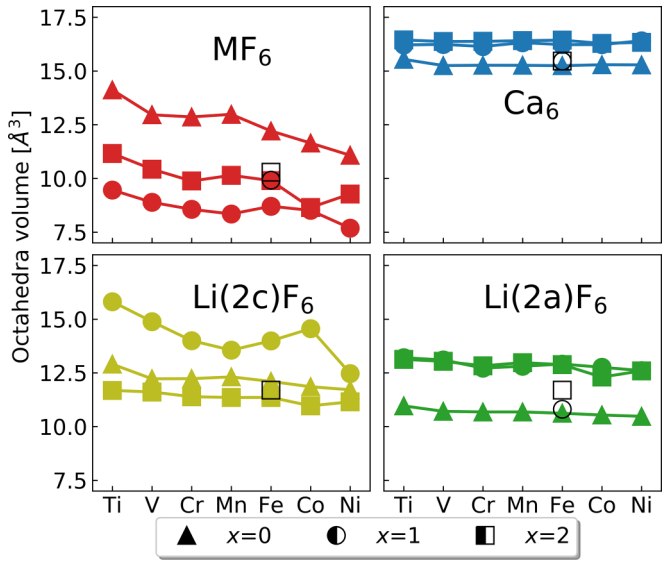

FIG. 4. Absolute volumes of the MF_6, LiF_6, and CaF_6 octahedra for the magnetic ground-state structures at $U = 4$ eV. The experimental results by de Biasi *et al.* [18] for Li_xCaFeF_6 are shown with open symbols. The scale of the y axis is the same for all the plots. Lines between data points serve as guide for the eye.

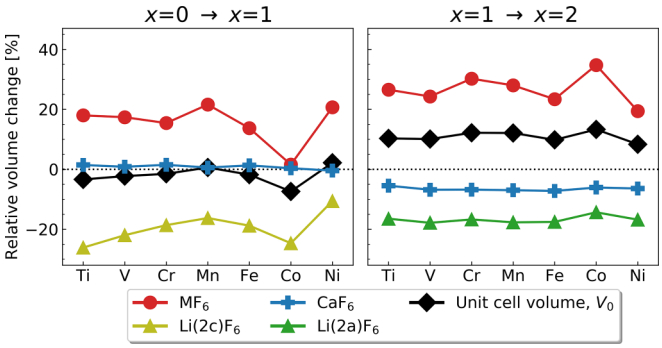

FIG. 5. Relative volume changes of the MF$_6$, LiF$_6$, and CaF$_6$ octahedra for the ground states obtained for $U = 4$ eV. For clarity only the changes of the Li octahedra, which are occupied in the corresponding lithiation step, are shown. Lines between data points serve as guide for the eye.

at $x = 1$ show a good agreement between the calculations of this work and the experimental results. For the higher Li concentration, however, especially the volume of the FeF$_6$ octahedron volume was measured to be much lower than the calculated one.

In Fig. 5 the relative volume changes of the fluorine octahedra in the two lithiation steps are displayed. For all the considered 3d TM elements M, the volumes of the octahedra around the Li sites that become occupied during the two lithiation steps get smaller. This is because of a reduction of the repulsion of the negatively charged fluorine anions of a F$_6$ octahedron, when a positively charged Li ion occupies its center. For the step from $x = 0$ to $x = 1$, the volume changes of the LiF$_6$ (2c) octahedra behave qualitatively similar along the 3d series as the volume changes of the MF$_6$ octahedra, which is due to shared F-F edges between them (cf. Fig. 1). In the second lithiation step the LiF$_6$ (2a) octahedra become occupied, which also share F-F edges with the MF$_6$ octahedra. However, they also share their top and bottom faces (in the [0001] direction) with two CaF$_6$ octahedra. This leads to a less pronounced correlation between MF$_6$ and LiF$_6$ (2a) octahedra.

The CaF$_6$ octahedra hardly change their volume in the first lithiation step, independent of the element M. However, in the second lithiation step, there is a nearly constant contraction by about 5–7% of the volumes of CaF$_6$ octahedra for all the considered M ions.

The relative change of the unit-cell volume of the colquiriite crystal, $\Delta V_0^{(\mathrm{rel.})} = (V_0[x+1] - V_0[x])/V_0[x]$, is also displayed in Fig. 5. In the first lithiation step (from $x = 0$ to $x = 1$), $\Delta V_0^{(\mathrm{rel.})}$ adopts negative values between 0 and −7% for most of the considered compounds or values slightly above zero for M = Mn and M = Ni. Especially for M = Mn, a remarkably small volume change of 0.5% indicates indeed a ZS behavior. For most of the compounds, volumes are compared between ground states, which have the same spin state (mainly HS, cf. Table II). Only for Li$_x$CaCoF$_6$ (HS to LS) and Li$_x$CaNiF$_6$ (LS to HS) is there a concomitant change of the magnetic ground state. For M = Co, this transition causes the pronounced deviation of the volume change to a negative value of −7.3%, more negative than the values of the other systems, in which no such transition between magnetic states takes place. For M = Ni, the different magnetic ground states do not lead to such a pronounced effect.

In the second lithiation step (from $x = 1$ to $x = 2$) all of the volume changes of the unit cells are positive within a range of about 8.5–12%. Only the compound containing Co exhibits a LS-to-HS transition, which results in a slightly higher value of 13.3% compared to the other M cations. The large relative change of the CoF$_6$ octahedra in this lithiation step stems from its volume at $x = 1$ being small compared to the volumes of the other MF$_6$ octahedra, while the absolute change of the octahedra volume is comparable to others (cf. Fig. 4).

The increasing volumes of the MF$_6$ octahedra affect the unit cell volumes, which can be seen from the qualitatively similar shapes of the red and black curves. The volume expansion of the MF$_6$ octahedra by up to 20% must be, at least partially, compensated by other effects to obtain the overall negative or very small positive changes of the unit-cell volumes. The joint effect of the local volume changes of the different octahedra on the total unit-cell volume of the colquiriite structure will be discussed in Sec. IV C. The absolute volumes (V_0) of the unit cells for all compounds and U values are listed in the supplemental material [54].

C. Theoretical capacities and voltages

To assess the suitability of the colquiriit compounds as active cathode materials, we calculated their theoretical capacities and voltages. The capacity is given by the maximum ionic charge which can be stored in the compounds (here two Li$^+$ ions per formula unit) with respect to its mass (gravimetric capacity) or equilibrium volume (volumetric capacity). Considering the total theoretically accessible lithiation range ($x = 0$ to $x = 2$), the gravimetric (volumetric) capacitities lie in the range of 222.6–233.4 mAh/g (240.9–263.3 mAh/cm^3) if referenced to the masses (equilibrium volumes) of the colquiriite compounds at $x = 2$. In comparison, the corresponding capacities of Li$_x$CoO$_2$ (LCO) are 273.8 mAh/g (339.1 mAh/cm^3) in the range $x = 0$ to $x = 1$. However, the cyclability of LCO is known to be restricted to the range $0.5 \leqslant x \leqslant 1$, reducing the capacity accordingly to 137 mAh/g [62]. The voltages can be determined from the total energies of the compounds [63], which we obtained from our DFT + U calculations. The voltages, referenced against the oxidation potential of metallic lithium, are displayed in Fig. 6 separately for the two lithiation steps. For all considered compounds, the voltage decreases from the first to the second lithiation step. This is in accordance with the finding that the occupation of the WP 2c in the first step is energetically more favorable than the occupation of the WP 2a in the second step. Our calculated voltage for the intercalation step from CaCoF$_6$ to LiCaCoF$_6$ of 5.6 V is in good agreement with the value reported by Koyama *et al.* (5.80 V) [17]. Koyama *et al.* attributed this relatively high voltage, e.g., compared to the value of 4.2 V for Li$_x$CoO$_2$, to the higher electronegativity of fluorine compared to oxygen. In line with this argument several considered compounds show higher voltages when compared to oxides utilizing the same redox couple (Ni^{4+}/Ni^{3+}: 4.3 V for Li$_x$NiO$_2$; Mn^{4+}/Mn^{3+}: 3.4 V for Li$_x$NiO$_2$ [59]). Only based on the calculated voltages, one could also imagine

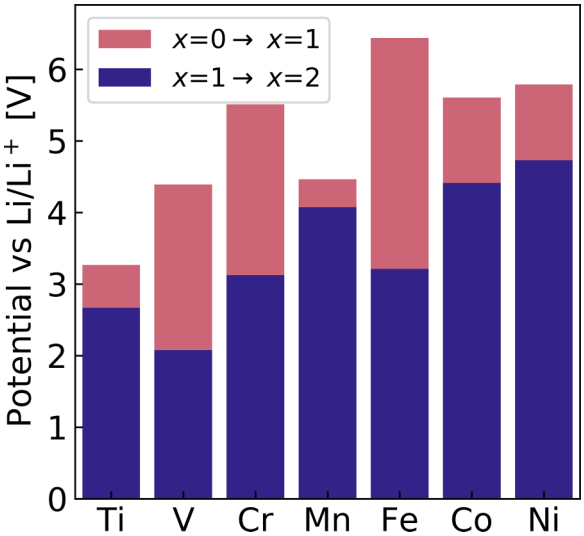

FIG. 6. Theoretical voltages of the Li_xCaMF_6 compounds for the two lithiation steps, $x = 0$ to $x = 1$ and $x = 1$ to $x = 2$.

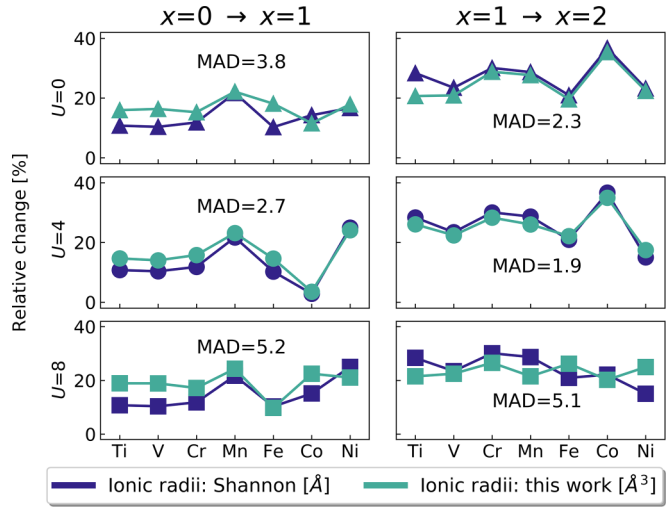

FIG. 7. Comparison of the lithiation induced relative changes of ionic radii from Shannon and from the calculations performed in this work. The three panels on the left (right) display the results for the first (second) lithiation step. The U correction on the M cations increases from top to bottom. Inserted into each panel is the MAD between the two sets of ionic radii changes.

a cell with Li_xCaTiF_6 as the anode cycled against Li_xCaFeF_6 as the cathode, resulting in about 3 V in the Li range $x = 0$ to $x = 1$. The voltage would, however, drop to an unfavorable small value for the second lithiation step.

IV. DISCUSSION

A. Choice of the U parameter

The oxidation number of the electrochemically active $3d$ TM cation decreases when lithium ions are inserted into the colquiriite-type crystal structure and the cations have different ionic radii at different oxidation states. In a simple picture, in which the bond length between two ions is the sum of their ionic radii, the relative change in ionic radius, $\Delta r^{(\mathrm{rel.})}$, can be related to the relative change of the MF_6 octahedron volume, $\Delta V^{(\mathrm{rel.})}$ (the derivation is presented in the supplemental material [54]):

$$\Delta V^{(\mathrm{rel.})} = [\alpha \Delta r^{(\mathrm{rel.})}]^3 + 3[\alpha \Delta r^{(\mathrm{rel.})}]^2 + 3\alpha \Delta r^{(\mathrm{rel.})}. \quad (1)$$

Here $\alpha = r_0/r_0 + r_L$ relates the change in ionic radius to the change in bond length, with r_0 and r_L being the ionic radius of the M cation in the initial state and the ionic radius of the ligand, F^-, respectively. The ionic radius of fluorine is 1.3 Å for a threefold coordinated ion in the charge state 1− and the typical values for the ionic radii of $3d$ TM lie in the range of 0.5 and 0.8 Å. Therefore α as well as $\Delta r^{(\mathrm{rel.})}$ both are small (<1), and the change in volume of the octahedra can be approximated by the last, linear term of the right-hand side of Eq. (1).

We choose the ionic radius to select an appropriate value for U because of its experimental availability and the established linear correlation to the change in MF_6 octahedron volume, an important quantity for the investigation of local and global volume changes due to Li insertion. For all our considered cations in their oxidation states 4+, 3+, and 2+, the ionic radii derived from experimental data of mineral structures, with the different magnetic spin states taken into account, were compiled by Shannon [49]. We derived the corresponding ionic radii from the bond lengths in our calculated ground-state crystal structures. Figure 7 compares the change in Shannon ionic radii to the change of our calculated ionic radii for the two lithiation steps and the three considered U values. Overall, the change in calculated radii fit well with the change in Shannon radii. For $U = 0$ eV and $U = 4$ eV, they even follow the same trend along the $3d$ series of the M cations, with a slight deviation only for $M =$ Fe and $M =$ Co in the first lithiation step for $U = 0$ eV. For $U = 8$ eV, the calculated values exhibit the strongest differences to the experimental ones, especially for the second lithiation step. In order to further quantify the agreement between the two sets, we calculated the mean absolute deviation (MAD) for each set of data points, which is displayed for each combination of lithiation step and U value in Fig. 7.

For both lithiation steps the MAD is lowest for $U = 4$ eV and for that value the overall trend along the series of M ions is well reproduced. This is in good agreement with other computational works on $3d$ TM fluorides: A value of 4 eV lays well in the range of previously used U corrections (e.g., 5 eV for Fe in FeF_3 [64], 4 eV for Ni and 5 eV for Co in $AgMF_4$ ($M =$ Ni, Co) [65], 2.4 eV for Ti and 5.0 eV for Fe ions in Na_2TiFeF_7, and 4 eV for Mn in $LiMn_2O_4$ [66]).

B. Changes in ionic radii along the $3d$ TM series

As described in Sec. III, the magnitude of volume changes of the colquiriite-type crystal structure on lithiation significantly depends on the species and size of the TM ion. Similar findings were reported by Ariyoshi *et al.* for solid solutions of $Li[Ni_{1-x-y}Co_xMn_y]O_2$ with $0 \leqslant x \leqslant 1$ and $0 \leqslant y \leqslant 1$ [67], where the ratio of the different TM species strongly influences the volume change in the lithiation process. Obviously, for both ligand elements $L = O$ and $L = F$, the volume changes of the ML_6 octahedra is correlated with the changes of the

ionic radii of the M ions. TM cations in lower oxidation states have larger ionic radii since the electrons are less strongly attracted by the smaller positive ionic charge. Therefore, the change in ionic radius is always positive with increasing Li concentration. The larger radii increase the bond lengths between the TM cations and the surrounding anions and, accordingly, the corresponding volumes of the coordination octahedra. Therefore, in the following, we first discuss the changes in ionic radii along the $3d$ TM series according to the ligand field theory (LFT) before we connect the local volume changes of the octahedra surrounding the cations with the global volume changes of the crystal structures in Sec. IV C.

According to the LFT, nine orbitals of the central TM cation can be involved in bonding in an octahedral coordination. For $3d$ TM, the involved atomic orbitals (AOs) are the $3d$, $4s$, and $4p$ orbitals. The $4s$ and the $4p$ orbitals have the symmetry a_{1g} and t_{1u}, respectively. The $3d$ orbitals are split into two symmetry groups, denoted e_g ($d_{x^2-y^2}$ and d_{z^2}) and t_{2g} (d_{xy}, d_{xz}, d_{yz}). In σ bonding, six orbitals of the ligands (for fluorides: one $2p$ orbital per fluorine) form symmetry adapted linear combinations (SALCs), which can be split into three symmetry groups: e_g, a_{1g}, and t_{1u}. In order to overlap (i.e., to form a σ bond) the AOs of the central cation and the SALCs must have the same symmetry. With the exception of the t_{2g} orbitals, this is fulfilled for all AOs and SALCs.

The t_{2g} can form π bonds with another set of SALCs of the ligands (formed by the other two $2p$ orbitals), which have the t_{2g} symmetry [68]. In general, the t_{2g} orbitals could also interact with t_{2g} orbitals from other metal cations in the colquiriite structure. However, the MF$_6$ octahedra are not directly connected to each other (i.e., no TM cation is the next nearest neigbhor to another TM cation) and are separated by more than 5.1 Å in the (0001) plane. Along the [0001] direction they are separated by CaF$_6$ octahedra, whose central cations have no d orbitals to form π bonds.

In summary, the orbitals with symmetry groups e_g, a_{1g}, and t_{1u} form σ bonding and antibonding (indicated by an asterisk) orbitals. The orbitals with symmetry group t_{2g} form π and π^* orbitals. All the bonding orbitals are occupied by the number of electrons corresponding to the number of $2p$ electrons of the F$^-$ ligands. The next orbitals that can be occupied are the antibonding t_{2g}^* and the e_g^* orbitals [69]. They are occupied by the number of electrons corresponding to the number of $3d$ electrons of the central TM. In general, antibonding orbitals increase the bond length. The t_{2g}^* form weaker π bonds compared to the e_g^* σ bonds. Therefore, the occupation of the former increases the M-F bond length to a lower extent. This has already been reported in other works, concerning $3d$ TM cathode materials [15,70]. As described in the context of Eq. (1), the M-F bond lengths are linearly related to the ionic radii of the M cations and to the MF$_6$ octahedron volumes.

We first discuss the relative change of the octahedron volumes during the first lithiation step for each M cation, as plotted in the left panel of Fig. 5. Figure 8 schematically depicts the formal spin configurations in the different oxidation states corresponding to the ground states obtained in the calculations (cf. Table II). For Ti, V, and Cr, the additional electron of the first inserted Li atom occupies one of the previously empty t_{2g}^* orbitals. For Mn, however, one of the e_g^* orbitals becomes filled, which results in a considerable increase of

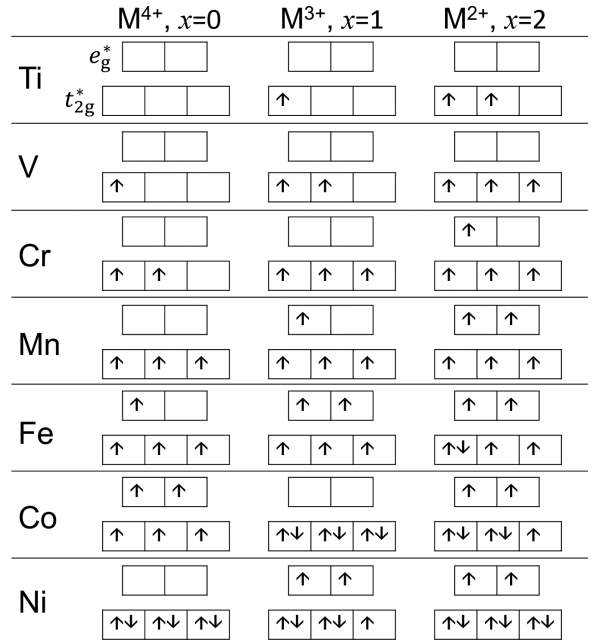

FIG. 8. Formal $3d$ orbital occupations for the three oxidation states of the $3d$ TM cations M in their respective ground states corresponding to the different Li concentrations x. Along the series from Ti to Fe, the ground states are always magnetic HS states. The magnetic states of Co (Ni) follow the sequence HS → LS → HS (LS → HS → HS) with increasing x.

the ionic radius. For Fe the change is again smaller, because in Fe^{4+} there was formally already one e_g^* orbital occupied and therefore the relative change due to the second e_g^* orbital becoming occupied is not as large.

The small volume change of the CoF$_6$ octahedron (1.6%) can be explained by the fact that for $x = 0$ the HS state is energetically preferred, while for $x = 1$ it is the LS state. This means that for $x = 0$ both e_g^* orbitals are singly occupied, while for $x = 1$ all three t_{2g}^* orbitals are doubly occupied by the six electrons. This relocation of the electrons nearly completely compensates the effect of the additional electron, which increases the ionic radius.

Ni (with formally 6 [Ni^{4+}] or 7 [Ni^{3+}] $3d$ electrons) exists in the LS state for $x = 0$ and in the HS state for $x = 1$. Therefore, at $x = 0$ all t_{2g}^* orbitals are doubly occupied and at $x = 1$, both e_g^* orbitals are singly occupied. As in the case of Mn, this also leads to a larger volume change of the M octahedron.

Corresponding arguments can be applied for the second lithiation step. The Cr and Co octahedra are expected to yield the largest positive changes, because for both systems previously empty e_g^* orbitals become occupied, which is reflected by the data points. The octahedron around Mn has a comparably large volume change, too, since here the second e_g^* orbital becomes occupied.

To strengthen the arguments made above based on the LFT, we relate them to the results of electronic structure calculations for site- and orbital-projected densities of states (PDOS) of the $3d$ orbitals of the TM ions. Figure 9 illustrates that for Li$_x$CaMnF$_6$ the charges obtained by integrating the PDOS up to the energy of the highest occupied level are for

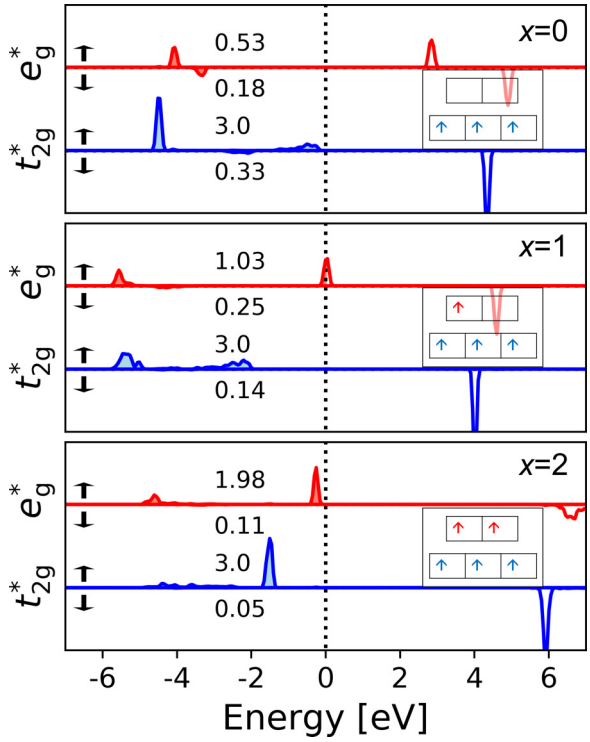

FIG. 9. Site- and orbital-projected densities of states of the t_{2g}^* and e_g^* orbitals of Mn in Li_xCaMnF_6, calculated with $U = 4$ eV. The insets sketch the expected formal distributions of the $3d$ electrons in the high-spin states (ground states for Li_xCaMnF_6) among the two orbital groups according to the LFT. The energies are referenced to the Fermi energy (dotted vertical lines). The numbers of electrons (or charges in units of the elementary charge) obtained by integrating over the occupied states in each orbital group and spin channel are written next to the corresponding curves.

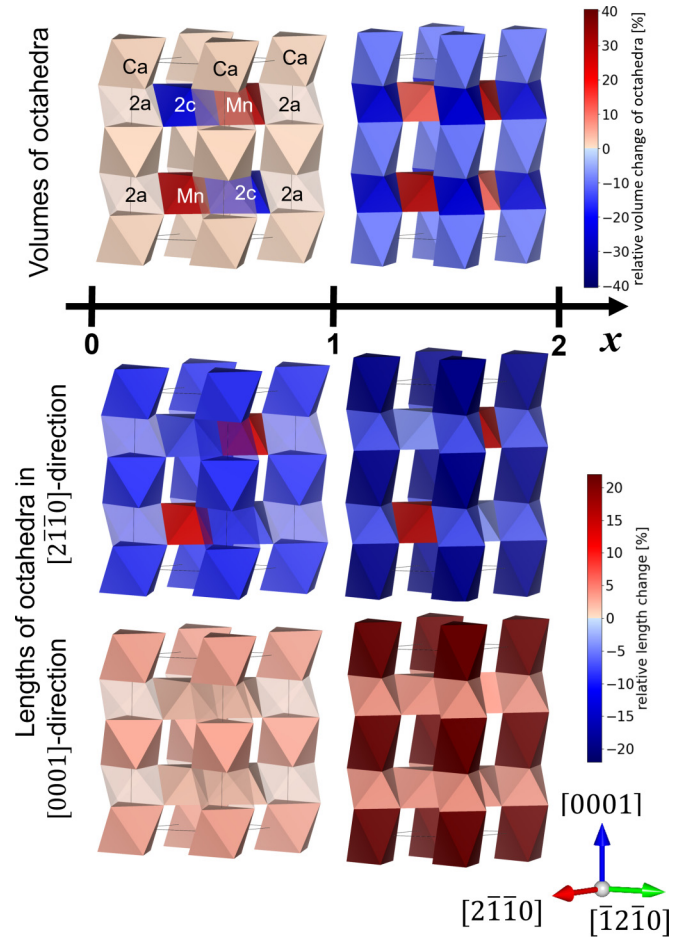

FIG. 10. Change of structural parameters of Li_xCaMnF_6 during the two lithiation steps. The upper two structures display the change in the octahedra volumes while the central and lower panels show the length changes of the octahedra along the lattice directions. Transparent octahedra represent octahedral sites that are not occupied. In the top left structure the Ca and Mn octahedra are labeled by the central cation and the lithium octahedra are labeled with the respective Wyckoff position.

both spin channels in good agreement with the formal charges expected from the LFT. The largest deviation is obtained for the e_g^* orbitals at $x = 0$ which show nonzero occupations in both spin channels. However, they are expected to be empty according to the LFT. We can attribute this small mismatch to some electronic hybridization interaction of the well localized $3d$ orbitals with the more delocalized, formally empty $4s$ and $4p$ orbitals. Therefore, a small fraction of the electron density gets projected onto atom-centered partial waves of d-orbital symmetry in the calculation and integration of the PDOS.

In the first lithiation step, the state in the spin-up channel of the e_g^* orbital, which is unoccupied at $x = 0$, shifts towards the Fermi level and becomes partially occupied at $x = 1$. In the second lithiation step, this state is shifted below the Fermi level and is then completely occupied. This trend agrees with the LFT and supports the validity of the arguments made above.

C. Effects of local volume changes on the volume change of the unit cell

To understand how the volume of the unit cell of the crystal is affected by the local volume changes of the fluorine coordinated octahedra around the different cations, we analyze the structural changes during lithiation with respect to the location of the octahedra and to their connections to each other in the colquiriite structure.

In Sec. III B we describe that the MF_6 octahedra swell in the first lithiation step, whereas the F_6 octahedra around the 2c sites, on which the Li ions are placed, shrink (cf. Fig. 5). This is shown schematically for Li_xCaMnF_6 in Fig. 10 (upper left structure). MF_6 and LiF_6 (2c) octahedra are located next to each other in the (0001) plane and are connected by a common edge. This leads to an elongation of both types of octahedra in the [0001] direction by the same amount, while the edge lengths in the in-plane directions ([2$\bar{1}\bar{1}$0] and [$\bar{1}$2$\bar{1}$0]) change oppositely for MF_6 and LiF_6 octahedra (lower left two structures in Fig. 10). For the series of considered compounds, these compensating effects lead to changes of the unit cell lattice parameter a between -4.2% and -1.0% and c between 0.9% and 2.6%. All values for the lattice parameters are summarized in the supplemental material [54]. For M = Mn the deformations along the different crystallographic directions compensate each other in such a way that the volume change

of the whole unit cell is less than 1%. Although the changes in lattice parameters a and c have different signs and magnitudes (-1.0% and 2.6%, respectively), which could lead to stresses in a confined single crystal material, we would expect an averaging out of the different expansions/contractions to some extent in a polycrystalline material and at the corresponding grain boundaries.

The volume change for Li_xCaCoF_6 of -7.4% that we find deviates considerably from the value of -0.4% reported by Koyama *et al.* [17]. The difference may at least partially be attributed to the inclusion of spin polarization and the application of a U correction in our work, which are both essential to get different magnetic states related to different oxidation states of the electroactive M cations, as discussed before. Spin-polarization and electron-correlation effects were not yet taken into account in the work of Koyama.

For the lithiation step from $x = 1$ to $x = 2$ the unit-cell-volume changes are positive for all the considered compounds and larger in magnitude, although the MF_6 octahedra and the LiF_6 octahedra behave similarly as for $x = 0$ to $x = 1$. The former swell and the latter shrink. This again leads to a compensation effect resulting in changes of the lattice parameter a between -0.6 and $+0.6\%$ for the set of considered compounds in the second lithiation step.

However, the increase of the lattice parameter c is more pronounced and leads in total to volume changes of the unit cells between 10% and 15% as displayed in Fig. 5 (right panel). This can be explained as follows: First, one can see in Fig. 10 that the MF_6 octahedra expand due to the oxidation in all three lattice directions $[2\bar{1}\bar{1}0]$, $[\bar{1}2\bar{1}0]$, and [0001]. The elongation in [0001] direction is transferred with the same extent to the neighboring LiF_6 (2c) and LiF_6 (2a) octahedra in the (0001) plane due to their edge connections (Fig. 10, bottom right structure). The occupation of the 2a positions by Li leads to a reduced electrostatic repulsion among the six surrounding F anions and an overall shrinkage of the LiF_6 (2a) octahedra. But since these increase in [0001] direction, the shrinkage in volume can only be realized by a reduction of the edge lengths in the $[2\bar{1}\bar{1}0]$ and $[\bar{1}2\bar{1}0]$ lattice directions. This is possible because there are no constraints imposed by the MF_6 octahedra for this structural adaption.

The top and bottom faces of the LiF_6 (2a) octahedra in the [0001] direction are shared with the CaF_6 octahedra, which accordingly also shrink in the $[2\bar{1}\bar{1}0]$ and $[\bar{1}2\bar{1}0]$ directions together with the LiF_6 (2a) octahedra.

Since the Ca cations do not change their oxidation state, no change in the average Ca-F bond length should occur. The trade-off between the reduced areas of the top and bottom faces of the Ca octahedra and the resistance against shorter Ca-F bonds results in an elongation of the CaF_6 octahedra along the [0001] lattice direction. This can be accomplished by the colquiriite crystal structure up to a certain extent since the CaF_6 octahedra are not constrained by other octahedra in this direction. A complete compensation, however, cannot be achieved, leading to a volume reduction for all CaF_6 octahedra (see Fig. 5).

The elongation of octahedra along the [0001] lattice direction yields changes in the c lattice parameter of the unit cell between 11.2% and 11.8% for the different M occupations and therefore an increase of the unit-cell volumes. The variation of the values for c is less than for a and also less than the change in c during the first lithiation step. In the second lithiation step the influence of the type of M cation on the volume change appears to be less pronounced than in the first lithiation step.

The theoretical calculated gravimetric capacity of 119.8 mAh/g of Li_xCaFeF_6 for the second lithiation step ($x = 1$ to $x = 2$) is in good agreement with the measured capacity of 112 mAh/g for the lithiation range from $1 \leqslant x \leqslant 1.8$ [18]. Also, our calculated value for the equilibrum voltage of 3.2 V lies well in the range of the measured voltages of 2.0–4.5 V. However, the calculated volume changes do not agree with the experimentally measured volume changes of $\Delta V_0^{(\mathrm{rel.})} \leqslant 0.5\%$. In line with the experimental results, we obtained Fe^{3+} octahedra (9.9 Å^3) with smaller volumes as the LiF_6 (2a) octahedra (10.8 Å^3), but in contrast to the experimental results we found at $x = 2$ larger octahedra around the Fe^{2+} (10.3 Å^3) than around the now-occupied Li ions (11.7 Å^3), cf. Fig. 4. In addition, the stretching of the Ca octahedra during the second lithiation step was not reported by de Biasi *et al.* Note that the cell volumes (and therefore the relative volume changes) only show a weak dependence with the used U correction, as long as the same magnetic states are stable (all equilibrium volumes are given in the supplemental material [54]). For Li_xCaFeF_6 the maximum difference in cell volumes for the same Li concentration amounts to 3.9 Å^3 for $x = 1$ with volumes between 229 Å^3 ($U = 8$ eV) and 233 Å^3 ($U = 0$ eV). Therefore the deviation to the experimental results cannot be attributed to an inappropriate choice of the U correction value. This leads us to the conclusion that the experimentally observed ZS behavior in Li_xCaFeF_6 cannot fully be understood as a single-crystal phenomenon. Other possible effects that result in a measured low volume change may be caused by Li ions at grain boundaries, other charged point defects (e.g., cation vacancies), or amorphous surface and interface layers.

V. CONCLUSIONS

We present a systematic DFT + U investigation of volume changes in colquiriite-type crystalline compounds Li_xCaMF_6 with varying Li concentration. Considering on the M positions different cations along the series of 3d transition-metal elements of the periodic table, we explored the influence of a Hubbard U correction on the magnetic ground states of the compounds. By comparing ionic radii obtained from those ground-state structures to Shannon's ionic radii we determined an appropriate U value of 4 eV. Trends in local and global structural changes along the 3d series of the TM elements are elucidated by relating the electronic structure results to predictions of the LFT. We explain the connection of volume changes of the fluorine coordinated octahedra surrounding the cations to the change of the unit cell volume. All the different octahedra have partly constructive and partly compensating influences on the volume change of the crystal unit cell.

Due to the large volume increase of the MF_6 octahedra from M^{3+} to M^{2+} and the stretching of the Ca octahedra in the second lithiation step, the unit cell volume increases from $x = 1$ to $x = 2$ by approximately 10% for all structures. This is not in line with experimental results for Li_xCaFeF_6.

This discrepancy may originate from extended defects in polycrystalline microstructures, such as grain boundaries, which are not covered in the single-crystal model of this work.

From $x = 0$ to $x = 1$ the different volume changes of the MF$_6$ octahedra follow the trend of the change in ionic radii and determine the magnitude and sign of the change of the unit-cell volume. The trend along the 3d TM series can be explained by the successive occupations of the two orbital groups t_{2g}^* and e_g^* by the additional electrons of the inserted Li atoms.

We found in our work that Li$_x$CaMnF$_6$ is a promising ZS candidate for a LIB cathode material with a voltage and a theoretical capacity comparable to capacities of common cathode materials [71]. To the best of our knowledge, this compound has only been synthesized for $x = 0$ in another structure type, namely one of binary fluorides, VF$_3$ [72], and its stability in the colquiriite structure as well as its suitability as cathode material has not yet been experimentally investigated.

ACKNOWLEDGMENTS

This work was funded by the German Research Foundation (DFG, Grant No. EL 155/29-1). The authors acknowledge support by the state of Baden-Württemberg through bwHPC and the German Research Foundation (DFG) through Grant No. INST 40/575-1 FUGG (JUSTUS 2 cluster). Crystallographic drawings were created using the software VESTA [73].

[1] J. S. Edge, S. O'Kane, R. Prosser, N. D. Kirkaldy, A. N. Patel, A. Hales, A. Ghosh, W. Ai, J. Chen, J. Yang, J. Jiang, S. Li, M. C. Pang, L. B. Diaz, A. Tomaszewska, M. W. Marzook, K. N. Radhakrishnan, H. Wang, Y. Patel, B. Wu *et al.*, Lithium ion battery degradation: What you need to know, Phys. Chem. Chem. Phys. **23**, 8200 (2021).

[2] J. P. Pender, G. Jha, D. H. Youn, J. M. Ziegler, I. Andoni, E. J. Choi, A. Heller, B. Dunn, P. S. Weiss, R. M. Penner, and C. B. Mullins, Electrode degradation in lithium-ion batteries, ACS Nano **14**, 1243 (2020).

[3] X. Han, L. Lu, Y. Zheng, X. Feng, Z. Li, Z. Li, J. Li, M. Ouyang, and M. Ouyang, A review on the key issues of the lithium ion battery degradation among the whole life cycle, eTransportation **1**, 100005 (2019).

[4] R. Hausbrand, G. Cherkashinin, H. Ehrenberg, M. Groeting, K. Albe, C. Hess, and W. Jaegermann, Fundamental degradation mechanisms of layered oxide Li-ion battery cathode materials: Methodology, insights and novel approaches, ChemInform **46**, 12 (2015).

[5] J. N. Reimers and J. R. Dahn, Electrochemical and in situ X-ray diffraction studies of lithium intercalation in Li$_x$CoO$_2$, J. Electrochem. Soc. **139**, 2091 (1992).

[6] X. Wang, Y. Sone, G. Segami, H. Naito, C. Yamada, and K. Kibe, Understanding volume change in lithium-ion cells during charging and discharging using in situ measurements, J. Electrochem. Soc. **154**, A14 (2007).

[7] R. Koerver, W. Zhang, L. de Biasi, S. Schweidler, A. O. Kondrakov, S. Kolling, T. Brezesinski, P. Hartmann, W. G. Zeier, and J. Janek, Chemo-mechanical expansion of lithium electrode materials—On the route to mechanically optimized all-solid-state batteries, Energy Environ. Sci. **11**, 2142 (2018).

[8] J. Wang and F. Hao, Experimental investigations on the chemo-mechanical coupling in solid-state batteries and electrode materials, Energies **16**, 1180 (2023).

[9] K. Zaghib, M. Armand, and M. Gauthier, Electrochemistry of anodes in solid-state Li-ion polymer batteries, J. Electrochem. Soc. **145**, 3135 (1998).

[10] T. Ohzuku, A. Ueda, and N. Yamamoto, Zero-strain insertion material of Li[Li$_{1/3}$Ti$_{5/3}$]O$_4$ for rechargeable lithium cells, J. Electrochem. Soc. **142**, 1431 (1995).

[11] B. Ziebarth, M. Klinsmann, T. Eckl, and C. Elsässer, Lithium diffusion in the spinel phase Li$_4$Ti$_5$O$_{12}$ and in the rocksalt phase Li$_7$Ti$_5$O$_{12}$ of lithium titanate from first principles, Phys. Rev. B **89**, 174301 (2014).

[12] H.-K. Tian, A. Chakraborty, A. A. Talin, P. Eisenlohr, and Y. Qi, Evaluation of the electrochemo-mechanically induced stress in all-solid-state Li-ion batteries, J. Electrochem. Soc. **167**, 090541 (2020).

[13] K. Ariyoshi, H. Yamamoto, and Y. Yamada, High dimensional stability of LiCoMnO$_4$ as positive electrodes operating at high voltage for lithium-ion batteries with a long cycle life, Electrochim. Acta **260**, 498 (2018).

[14] K. Ariyoshi, Y. Orikasa, K. Kajikawa, and Y. Yamada, Li$_2$Ni$_{0.2}$Co$_{1.8}$O$_4$ having a spinel framework as a zero-strain positive electrode material for lithium-ion batteries, J. Mater. Chem. **7**, 13641 (2019).

[15] X. Zhao, Y. Tian, Z. Lun, Z. Cai, T. Chen, B. Ouyang, and G. Ceder, Design principles for zero-strain Li-ion cathodes, Joule **6**, 1654 (2022).

[16] Y. Han, J. Hu, C. Yin, Y. Zhang, J. Xie, D. Yin, and C. Li, Iron-based fluorides of tetragonal tungsten bronze structure as potential cathodes for Na-ion batteries, J. Mater. Chem. **4**, 7382 (2016).

[17] Y. Koyama, I. Tanaka, and H. Adachi, New fluoride cathodes for rechargeable lithium batteries, J. Electrochem. Soc. **147**, 3633 (2000).

[18] L. de Biasi, G. Lieser, C. Dräger, S. Indris, J. Rana, G. Schumacher, R. Mönig, H. Ehrenberg, J. R. Binder, and H. Geßwein, LiCaFeF$_6$: A zero-strain cathode material for use in Li-ion batteries, J. Power Sources **362**, 192 (2017).

[19] T. Fleischer and R. Hoppe, Zur Rutilverwandtschaft: Zur Kenntnis von LiSrFeF$_6$[1]/On the knowledge of LiSrFeF$_6$, Z. Naturforsch. B **37**, 981 (1982).

[20] K. I. Schaffers and D. A. Keszler, Structure of LiSrAlF$_6$, Acta Cryst. C, **C47**, 18 (1991).

[21] Y. Yin and D. A. Keszler, Crystal chemistry of colquiriite-type fluorides, Chem. Mater., **4**, 645 (1992).

[22] Y. Yin and D. A. Keszler, Barium solubility in colquiriite fluorides, Mater. Res. Bull., **28** 1337 (1993).

[23] D. Klimm and P. Reiche, Nonstoichiometry of the new laser host $LiCaAlF_6$, Cryst. Res. Technol. **33**, 409 (1998).

[24] Y. Ono, K. Nakano, K. Shimamura, T. Fukuda, and T. Kajitani, Structural study of colquiriite-type fluorides, J. Cryst. Growth **229**, 505 (2001).

[25] M. Cadatal-Raduban, T. Shimizu, N. Sarukura, K. Takahashi, and T. Fukuda, Crystal growth of ultra-large MgF_2 and $LiCaAlF_6$ single crystals by a double-crucible Czochralski technique, J. Cryst. Growth **571**, 126260 (2021).

[26] S. Payne, L. Chase, H. Newkirk, L. Smith, and W. Krupke, $LiCaAlF_6$:Cr^{3+}: A promising new solid-state laser material, IEEE J. Quant. Electron. **24**, 2243 (1988).

[27] M.-H. Du and D. J. Singh, Electronic structure, small polaron, and F center in $LiCaAlF_6$, J. Appl. Phys. **112**, 123516 (2012).

[28] M. V. Luong, M. J. F. Empizo, M. Cadatal-Raduban, R. Arita, Y. Minami, T. Shimizu, N. Sarukura, H. Azechi, M. H. Pham, H. D. Nguyen, Y. Kawazoe, K. G. Steenbergen, and P. Schwerdtferger, First-principles calculations of electronic and optical properties of $LiCaAlF_6$ and $LiSrAlF_6$ crystals as VUV to UV solid-state laser materials, Opt. Mater. (Amsterdam) **65**, 15 (2017).

[29] T. Shimizu, M. V. Luong, M. Cadatal-Raduban, M. J. F. Empizo, K. Yamanoi, R. Arita, Y. Minami, N. Sarukura, N. Mitsuo, H. Azechi, M. H. Pham, H. D. Nguyen, K. Ichiyanagi, S. Nozawa, R. Fukaya, S.-ichi Adachi, K. G. Nakamura, K. Fukuda, Y. Kawazoe, K. G. Steenbergen *et al.*, High pressure band gap modification of $LiCaAlF_6$, Appl. Phys. Lett. **110**, 141902 (2017).

[30] U. Demirbas, Cr:Colquiriite Lasers: Current status and challenges for further progress, Prog. Quantum Electron. **68**, 100227 (2019).

[31] D. A. Pawlak, K. Wozniak, K. Shimamura, and T. Fukuda, Correlation between structural parameters of colquiriite structures, J. Cryst. Growth **233**, 699 (2001).

[32] M. van Schilfgaarde, I. A. Abrikosov, and B. Johansson, Origin of the Invar effect in iron-nickel alloys, Nature (London) **400**, 46 (1999).

[33] V. L. Moruzzi, P. M. Marcus, K. Schwarz, and P. Mohn, Ferromagnetic phases of bcc and fcc Fe, Co, and Ni, Phys. Rev. B **34**, 1784 (1986).

[34] A. Houari, S. F. Matar, and M. Belkhir, DFT study of magnetovolume effects in iron and cobalt nitrides, J. Magn. Magn. Mater. **322**, 658 (2010).

[35] W. Viebahn, Untersuchungen an quaternären Fluoriden $LiMe^{II}Me^{III}F_6$ Die Struktur von $LiCaAlF_6$, Z. Anorg. Allg. Chem. **386**, 335 (1971).

[36] F. D. Murnaghan, The compressibility of media under extreme pressures, Proc. Natl. Acad. Sci. USA **30**, 244 (1944).

[37] B. Silvi and P. d'arco, *Modelling of Minerals and Silicated Materials* (Springer, Dordrecht, 2002).

[38] V. Tyuterev and N. Vast, Murnaghan's equation of state for the electronic ground state energy, Comput. Mater. Sci. **38**, 350 (2006).

[39] G. Kresse and J. Furthmüller, Efficient iterative schemes for ab initio total-energy calculations using a plane-wave basis set, Phys. Rev. B **54**, 11169 (1996).

[40] J. P. Perdew, K. Burke, and M. Ernzerhof, Generalized gradient approximation made simple, Phys. Rev. Lett. **77**, 3865 (1996).

[41] G. Kresse and D. Joubert, From ultrasoft pseudopotentials to the projector augmented-wave method, Phys. Rev. B **59**, 1758 (1999).

[42] V. I. Anisimov, J. Zaanen, and O. K. Andersen, Band theory and Mott insulators: Hubbard U instead of Stoner I, Phys. Rev. B **44**, 943 (1991).

[43] S. A. Tolba, K. M. Gameel, B. A. Ali, H. A. Almossalami, and N. K. Allam, The DFT+U: Approaches, accuracy, and applications, in *Density Functional Calculations*, edited by G. Yang (IntechOpen, Rijeka, 2018), Chap. 1.

[44] B. Himmetoglu, A. Floris, S. de Gironcoli, and M. Cococcioni, Hubbard corrected DFT energy functionals the LDA+U description of correlated systems, Int. J. Quant. Chem. **114**, 14 (2013).

[45] C. A. Corrêa and K. Výborný, Electronic structure and magnetic anisotropies of antiferromagnetic transition-metal difluorides, Phys. Rev. B **97**, 235111 (2018).

[46] J. Kang, J. Ahn, H. Park, W. Ko, Y. Lee, S. Lee, S. Lee, S.-K. Jung, and J. Kim, Highly stable Fe^{2+}/Ti^{3+}-based fluoride cathode enabling low-cost and high-performance Na-Ion batteries, Adv. Funct. Mater. **32**, 2201816 (2022).

[47] K. Tada, M. Mori, and S. Tanaka, Spin contamination errors in DFT+U/plane-wave calculations for $LixFeF_3$ systems (x = 0-1), Chem. Lett. **50**, 1057 (2021).

[48] E. Di Lucente, M. Simoncelli, and N. Marzari, Crossover from Boltzmann to Wigner thermal transport in thermoelectric skutterudites, Phys. Rev. Res. **5**, 033125 (2023).

[49] R. D. Shannon, Revised effective ionic radii and systematic studies of interatomic distances in halides and chalcogenides, Acta Cryst. A **32**, 751 (1976).

[50] S. L. Dudarev, G. A. Botton, S. Y. Savrasov, C. J. Humphreys, and A. P. Sutton, Electron-energy-loss spectra and the structural stability of nickel oxide: An LSDA+U study, Phys. Rev. B **57**, 1505 (1998).

[51] H. J. Monkhorst and J. D. Pack, Special points for Brillouin-zone integrations, Phys. Rev. B **13**, 5188 (1976).

[52] C. L. Fu and K. M. Ho, First-principles calculation of the equilibrium ground-state properties of transition metals: Applications to Nb and Mo, Phys. Rev. B **28**, 5480 (1983).

[53] C. Elsässer, M. Fähnle, C. T. Chan, and K. M. Ho, Density-functional energies and forces with Gaussian-broadened fractional occupations, Phys. Rev. B **49**, 13975 (1994).

[54] See Supplemental Material at http://link.aps.org/supplemental/10.1103/PhysRevB.108.165140 for allcalculated volumes, lattice constants, magnetic moments of the TM ions and the derivaiton of Eq. (1).

[55] H. Jia, M. Horton, Y. Wang, S. Zhang, K. A. Persson, S. Meng, and M. Liu, Persona of transition metal ions in solids: A statistical learning on local structures of transition metal oxides, Adv. Sci. **9**, 2202756 (2022).

[56] A. Jain, S. P. Ong, G. Hautier, W. Chen, W. D. Richards, S. Dacek, S. Cholia, D. Gunter, D. Skinner, G. Ceder, and K. A. Persson, Commentary: The Materials Project: A materials genome approach to accelerating materials innovation, APL Mater. **1**, 011002 (2013).

[57] M. Bianchini, M. Roca-Ayats, P. Hartmann, T. Brezesinski, and J. Janek, There and back again—The journey of $LiNiO_2$ as a cathode active material, Angew. Chem. Int. Ed. **58**, 10434 (2019).

[58] N. Tsebesebe, K. Kgatwane, R. Ledwaba, and P. Ngoepe, Investigating the structural and electronic properties of $LiMO_2$ (M: Mn, Ni, Co) as potential cathode materials: A DFT study, J. Phys.: Conf. Ser. **2298**, 012010 (2022).

[59] A. Chakraborty, M. Dixit, D. Aurbach, and D. T. Major, Predicting accurate cathode properties of layered oxide materials using the SCAN meta-GGA density functional, npj Comput. Mater. **4**, 60 (2018).

[60] K. Saritas, E. R. Fadel, B. Kozinsky, and J. C. Grossman, Charge density and redox potential of $LiNiO_2$ using ab initio diffusion quantum Monte Carlo, J. Phys. Chem. C **124**, 5893 (2020).

[61] L. A. Mariano, B. Vlaisavljevich, and R. Poloni, Biased spin-state energetics of Fe(II) molecular complexes within density-functional theory and the linear-response Hubbard U correction, J. Chem. Theory Comput. **16**, 6755 (2020).

[62] D. Deng, Li-ion batteries: Basics, progress, and challenges, Energy Sci. Eng. **3**, 385 (2015).

[63] A. Urban, D.-H. Seo, and G. Ceder, Computational understanding of Li-ion batteries, npj Comput. Mater. **2**, 16002 (2016).

[64] R. Li, R. Li, S. Wu, Y. Yang, and Z.-Z. Zhu, Structural and electronic properties of Li-ion battery cathode material FeF_3, J. Phys. Chem. C **114**, 16813 (2010).

[65] M. A. Domański, M. Derzsi, and W. Grochala, Theoretical study of ternary silver fluorides $AgMF_4$ (M = Co, Ni, Cu) formation at pressures up to 20 GPa RSC Adv. **11**, 25801 (2020).

[66] B. Ramogayana, D. Santos-Carballal, K. P. Maenetja, K. T. Malatji, N. H. de Leeuw, and P. E. Ngoepe, A DFT+U-D3 study of the adsorption of hydrogen fluoride and ethylene carbonate on the niobium-doped (001), (011), and (111) surfaces of lithium manganese oxide, J. Electrochem. Soc. **169**, 090507 (2022).

[67] K. Ariyoshi, H. Yamamoto, and Y. Yamada, Relationship between changes in ionic radius and lattice dimension of lithium manganese oxide spinels during lithium insertion/extraction, Solid State Ionics **343**, 115077 (2019).

[68] G. Miessler and D. Tarr, *Inorganic Chemistry* (Pearson Education, London, 2004).

[69] J. S. Griffith and L. E. Orgel, Ligand-field theory, Q. Rev. Chem. Soc. **11**, 381 (1957).

[70] C. A. Marianetti, D. Morgan, and G. Ceder, First-principles investigation of the cooperative Jahn-Teller effect for octahedrally coordinated transition-metal ions, Phys. Rev. B **63**, 224304 (2001).

[71] N. Nitta, F. Wu, J. T. Lee, and G. Yushin, Li-ion battery materials: Present and future, Mater. Today **18**, 252 (2015).

[72] R. Hoppe and K. Blinne, Hexafluoromanganate IV der Elemente Ba, Sr, Ca und Mg, Z. Anorg. Allg. Chem. **291**, 269 (1957).

[73] K. Momma and F. Izumi, VESTA 3 for three-dimensional visualization of crystal, volumetric and morphology data, J. Appl. Cryst. **44**, 1272 (2011).